Helium Plasma Jet Interaction with Different Target Materials and the Plasma Characteristics on the Irradiation Area

Asma Begum[1*], Tatsuo Ishijima[2], Mohammad Rasel Pervez[2], Motawakkel Billah[3]

[1] Department of Physical Sciences, Independent University Bangladesh
E-mail: ablipi@iub.edu.bd, ablipi@gmail.com
[2] Kanazawa University, Japan
E-mail: ishijima@ec.t.kanazawa-u.ac.jp
raselpervez@stu.kanazawa-u.ac.jp
[3]Department of Natural Science; International University of Scholars
E-mail: billah@ius.edu.bd

Abstract

The experimental study on the dynamic behavior of helium atmospheric pressure plasma jet exposed on the surface of different conductivity is reported in this article. Electrical, optical, and gas dynamics characteristics are monitored using a high voltage probe, current probe, and imaging technique. The turbulence-free plasma jet length is estimated from the image of the plasma jet and correlated with the length estimated through the Electrohydrodynamic number (*Ehd* number). It has been shown that plasma species strongly modify the gas dynamics on the contact surface. The irradiation area on agar gel, metal, and Teflon is observed and the different flow regimes (free jet, stagnant region, and accelerating region) are identified. The irradiation area is significantly broadened for the polymer-like substrate and intensity is higher close to the stagnant region. The excited nitrogen and OH intensity are higher than the other observed chemical species on the target surface. The turbulence is higher near the outer radius of the irradiated surface, and it increases with operating voltage. The chemistry of the water changes with the presence of the metal probe inside the water.

Keywords: Atmospheric pressure plasma jet, surface modification, plasma jet-surface interaction

1. INTRODUCTION

The atmospheric pressure non-thermal plasma jet is a small device that functions in a wonderfully simple way, opening a wide variety of windows in the plasma industry and biomedical applications [1-5]. In recent years, temperature-sensitive surface modification [6-8] using non-thermal plasma is getting more attention. In most applications, plasma jets encounter metal, dielectric, polymer, and water. Low-temperature plasma processing is unique, as it can simultaneously change the substrate's surface characteristics and delivers the necessary plasma species for deposition. This non-thermal small-dimension plasma jet is more effective in small-scale surface modification than low-pressure plasma-driven surface modification. The interaction of the plasma jet with different surfaces is an important research area for the successful application of this plasma. Some research groups observed the plasma jet's interaction with metal and glass surfaces using the imaging technique [9-12]. The researchers are using in-liquid plasma (discharge inside the liquid) as an emerging technology for nanoparticle synthesis. The properties of the substrate have a huge effect on this small dimension, the transient plasma jet's characteristics, and its propagation phenomenon which indirectly affects the plasma application. Recently researchers have been actively working to understand the contact surface's effects on the gas jet flow [13-15]. It has been found that a conductor close to the jet front changes the shape and size of the jet [16]. Different research groups are working on the jet's characteristics while it is in contact with a dielectric or a conducting material [17-22]. Energy transfer to the substrate from the plasma is important in plasma processing. The spreading pattern of the plasma jet and the irradiation area on the different target materials are important for the application of the small-dimension plasma jet within the restricted area [23, 24].

This work investigates the dynamic behavior of the APPJ interacting with different substrate materials and the small-scale plasma jet's spreading on the substrates using electrical, optical, and chemical diagnostic techniques. We have estimated the plasma irradiation area on the substrate, the total charge flowing through the substrate, the different irradiation zone on the substrate, and the plasma species intensity along that irradiated area.

2. EXPERIMENTAL SET-UP

The schematic of the experimental setup is shown in Fig. 1(a). A copper High Voltage (HV) electrode is attached to the inner surface of a hollow quartz cylinder of 4.5 mm inner diameter. A quartz circular disk of diameter, *D* = 1 cm with a 1mm orifice at its center of the disk is attached to the cylinder's outlet, and a ring-shaped ground made of copper (*Diameter* = 3.5 mm) is attached to the outer surface of the disk keeping the orifice as the center (Fig. 1a). 99% pure helium gas flow is maintained through the cylinder using a digital flow meter. A parameterized bipolar pulse power supply with 0-20 kV peak-to-peak voltage with a pulse repetition rate of 10 kHz is used to ignite the jet. The pulse width is 20 µs and the off-voltage phase is 80 µs. The voltage-current waveform of the plasma jet is measured and recorded by Tektronix high voltage probe (P 6015A), current monitor probe (Pearson 2877), and digital oscilloscope [KEYSIGHT DSOX2004A Oscilloscope: 70 MHz, 2 GSa/s]. A Canon digital camera with a 2-millisecond exposure time is used to collect the discharge image. Ocean Optics USB 2000+ spectrometer (250-900 nm range) is used to collect the emission spectra. The helium flow dynamics were visualized by using a Schlieren system [SS100 (KATOKOKEN, Japan)]. This system consists of a VW-9000 ultra-fast camera (400 fps), a Xe-lamp of 75 W, and lenses with a focal length of 100 cm. The diameter of the pinhole is 1 mm, and the observation area is 100 mm in diameter.

In this experiment we have used copper plate (width = 1 mm, Area = 2.5 cm^2), agar gel (thickness = 2 mm, area = 9.42 cm^2), and Teflon (area = 2.5 cm^2) as target material. A circular copper disk of diameter, *D* = 2.3 cm connected to the ground is placed on the outer surface of the substrate and used to measure the charges passing through the target (Fig. 1c). The target attached to the metal probe is placed on an insulated stage. 10 ml of distilled water kept in a dielectric tube (*height = 2.5 cm, inner diameter = 1.8 cm*) was used as a water sample and a small metal plate connected to the ground was placed inside the liquid to measure the current through the water and to find the effect of this metal on the liquid chemistry during plasma treatment (Fig. 1c).

Chemical dosimetry based on terephthalic acid (TA) was used to measure the OH radicals

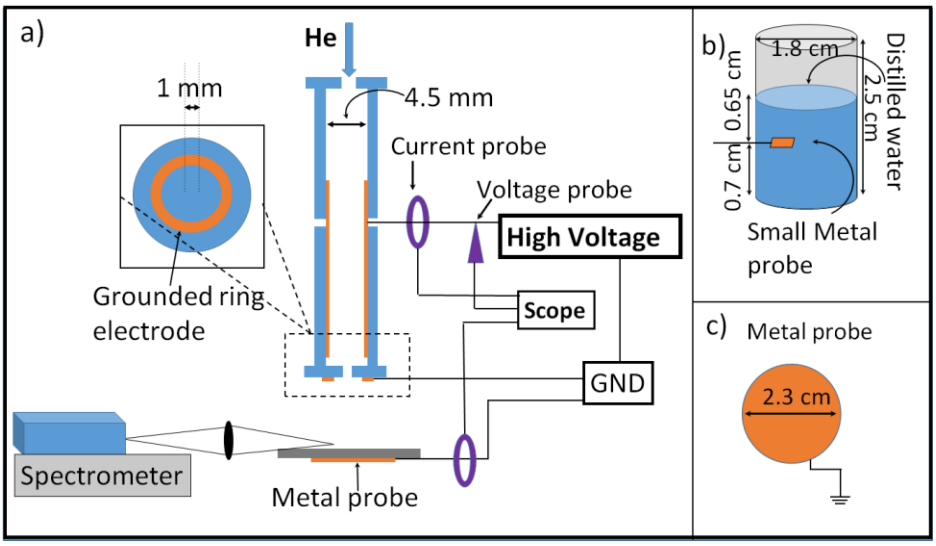

Figure 1. Experimental setup: a) Schematic diagram of the experimental setup, b) the water sample with small, grounded metal inside, c) Metal probe to measure the current through the substrate.

dissolved in the liquid. The OH radical converts terephthalic acid to 2-hydroxyterephthalic acid (HTA), which has been detected by fluorescence measurement, where the sample is irradiated by UV light at 315 nm. The production of OH radical and its chemical reaction with TA solution has given below [25].

$$\cdot OH + TA \rightarrow HTA$$

3. RESULTS and DISCUSSION

3.1 Identifying the Laminar Operating Regime

A current-voltage characteristic graph of the plasma cavity during the plasma "on" state is shown in figure 2a. During the positive voltage phase, the maximum current is 2 mA and during the negative voltage phase, the maximum current is 3 mA. A suitable operating parameter of the plasma jet is identified from the images (Figure 2b) taken for two different operating conditions: i) changing Gas Flow Rate (GFR) from 1 slm to 5 slm for the fixed applied voltage of 6 kV-p, and ii) changing applied voltage from 2 - 10 kVp-p for the fixed GFR of 2 slm. The length of the plasma jet increases until the GFR of 2 slm for the applied voltage of 6 kV (Fig, 2bi). Because of the different stresses active on the surface of the gas flow channel, at the higher gas flow rate turbulence is observed at the jet boundary and the tail of the plasma jet. At the higher GFR not only the turbulence but also the helical pattern in the plasma jet has been observed, which is also

reported in [26-31]. On the other hand, the length of the plasma jet reaches its maximum around the applied voltage of 9 kV for the GFR of 2 slm (Fig, 2bii). At the applied voltage of 10 kV,

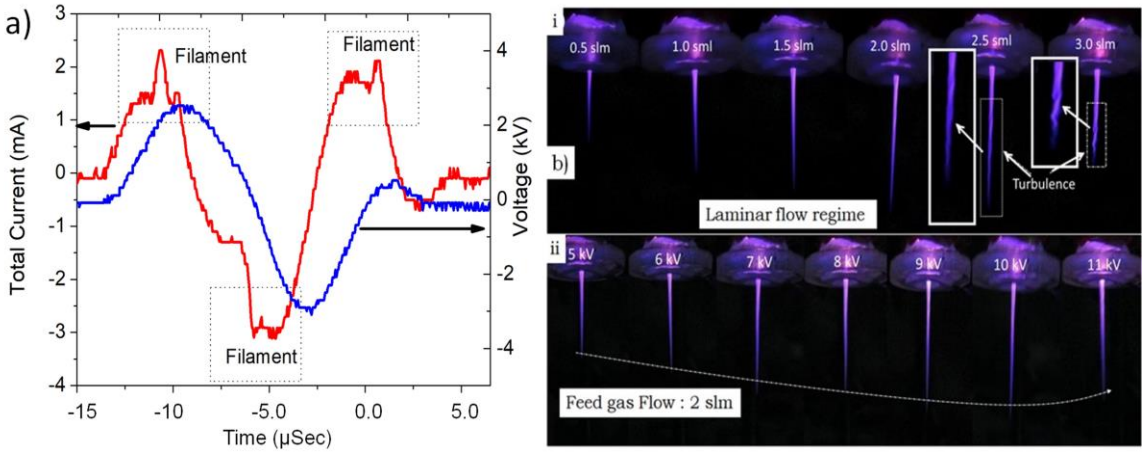

Fig. 2a) Applied voltage-total current graph of the plasma cavity, b) the length of the plasma jet changes with GFR and Applied voltage which gives the idea of the laminar flow regime.

several sparks were observed inside the plasma chamber. The suitable operating parameters for this experiment are the GFR of 1.75 slm and the applied voltage of 5.5 kV (p-p).

The diameter of the plasma jet decreases along the jet axis [32]. The shape of the plasma jet is related to the feed gas velocity, and thus the dynamic pressure of the flow channel. This pressure plays an important role in the spreading of the plasma jet on the substrate's surface. The gas jet broadens linearly along the axis by extensive exchange of momentum with the surrounding gas. Along the free jet zone, the gas jet velocity is [33-36],

$$v(0,z') = v_{nozzle}\left[1-\exp\left(-\frac{D/z'}{\sqrt{2}C}\right)^2\right]^{1/2} \qquad 1$$

Where, $v(0,z')$ is the axial gas velocity, D is the diameter of the nozzle, v_{nozzle} is the velocity at the exit point, C is a constant, depends on the diameter of the nozzle and its approximate value is 0.102, and z' is the position on the jet axis from the nozzle. The Helium density at Normal Temperature and Pressure (NTP) is 0.167 kg/m^3. The dynamic viscosity of helium gas is 1.98 x 10^{-5} Pa s [37]. Considering the nozzle diameter (1 mm) and helium gas flow rate (1.75 slm), Reynold's number at the nozzle is 516 which is much lower than the critical Reynold's number for helium's turbulent flow. The gas jet's velocity and the helium mole fraction along the jet axis were calculated using equation 1 is shown in Fig 3a. The laminar

plasma jet can be observed until 1.5 cm of the jet axis, measured from the nozzle. The substrate was placed 0.8 cm from the jet axis, where the gas velocity is around 31.5 m/s. The calculated Reynold's number is 227, which indicates the laminar flow of the gas. A new combined parameter, *Ehd* number, ($Ehd/(R_e)^2$) [38] is calculated to observe the effect of plasma current on the turbulence of the plasma jet shown in Fig 3b. Here, *Ehd*, the electrohydrodynamic force is defined by the relation,

$$Ehd = \frac{L^3 I_T}{\mu_i \rho_g \nu_g{}^2 A} \qquad 2$$

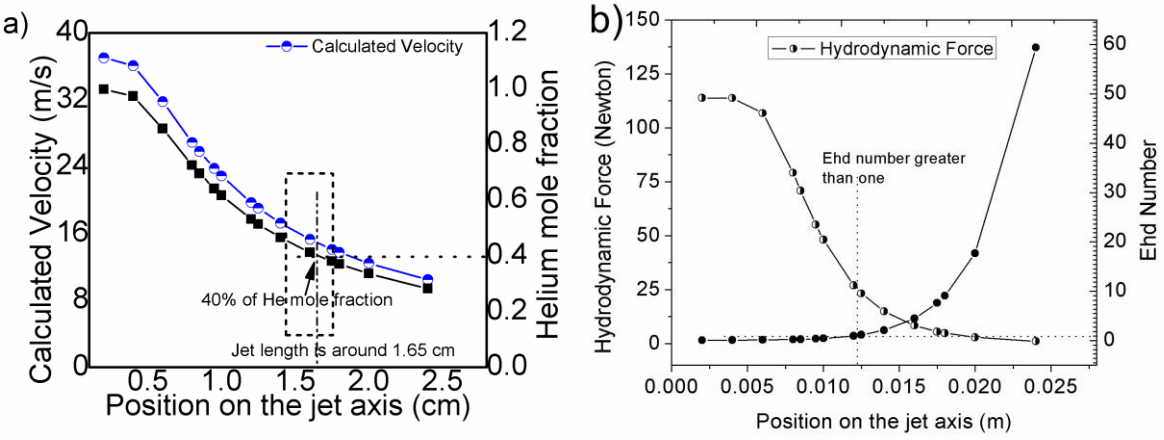

Fig. 3 a) The gas velocity and the helium mole fraction along the gas jet axis, b) Hydrodynamic force and the *Ehd* number Ehd/R^2 along the jet axis. This ratio crosses the number 1 at 1.25 cm of the jet axis.

where, L is the characteristic length, I_T is the total discharge current, μ_i is the ion mobility, ρ_g is the gas density, υ_g is the gas kinematic viscosity and A is the surface area of the collecting electrode. *EhD* number greater than 1 means the turbulence in the plasma jet. In our case turbulence was observed around 1.2 cm of the plasma jet. The hydrodynamic force ($= 0.5\rho_g v^2$) is also shown in figure 3b.

3.2 Effect of Substrate's Conductivity

3.2.1 Jet current passing through the substrate

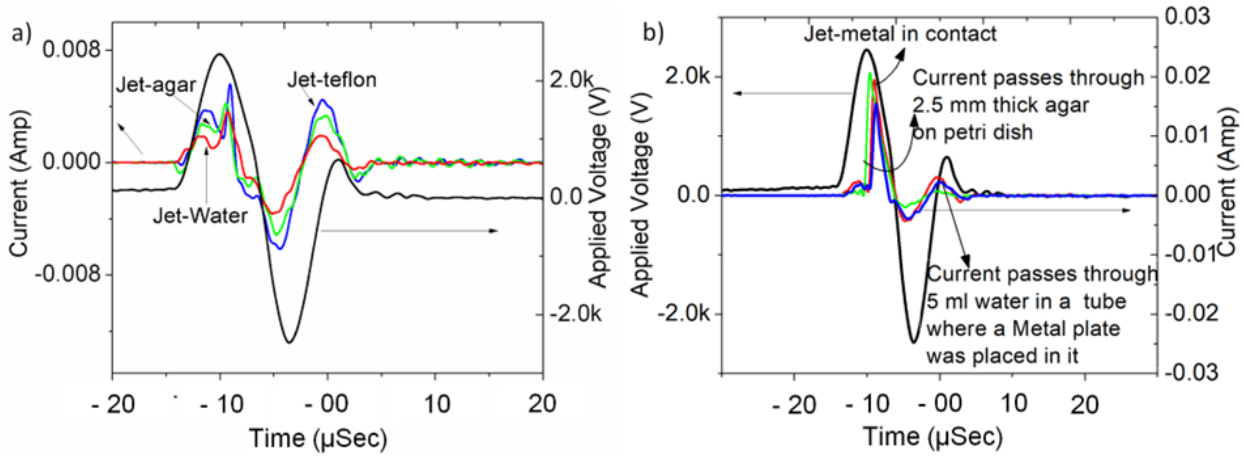

Fig. 4a) Current passing through the dielectric barrier in between substrate and probe, b) current passing through the substrate.

To discern the effects of the substrate's conductivity on the flow dynamics, first, we measured the current passing through the target/substrate. A circular metal disk (metal probe) connected to the ground was placed underneath the substrate to measure the current flowing through the medium. Figure 4a shows the current passing through the probe when the probe is attached to the agar gel-containing petri dish, Teflon, and the water-containing tube. Figure 4b shows the current passing through the probe when it is placed beneath the agar gel, copper plate, and inside the water (Fig. 1c). The maximum current is much lower when the probe is placed remotely (probe is attached to the substrate container) and under the Teflon, compared to the current passing through metal, agar gel, and water when the probe is directly in contact with the substrate. The current-time waveform shows that there is a sharp increase in the current pulse during the 1st positive voltage pulse. The maximum positive currents are 20 mA, 19 mA, 15 mA, and 5.4 mA for metal, agar gel, water, and Teflon, respectively (figure 4b). The conductivity of these materials decreases from the copper to the Teflon in the same manner. For the metal target, the current pulse rises a little earlier than the other two targets, it's because of the higher conductivity of this material. The total charges passing through the materials are in the same order (~10^{-8} C).

The calculated total charge per pulse from the current is also shown in Table-I. The total charge per voltage pulse is calculated by integrating the current curve for all different set-ups are, jet –

metal: 4.42x10^{-8} C, jet–water: 2.35x10^{-8} C when the metal probe is inside, and 1.15x10^{-8} C when the metal probe is on the outer surface, and jet–agar: 4.38x10^{-8} C, when agar gel containing Petri dish attached to the probe: 1.2x10^{-8} C. Even though the conductivity of the agar gel is much lower than copper, the total charge passing through this is almost the same as copper. It is because of the porosity of the agar gel. As the agar gel is soft, the gas jet creates a dimple on the surface which decreases the thickness of the agar gel. The total charge calculated for jet-Teflon interaction is 1.3x10^{-8} C.

Table I: Total charge and maximum current passes through the target in different set-up

Contact surface	**Total charge (C)**
Metal	4.43x10^{-8}
Ager gel – I	4.35 x10^{-8}
Water – I	2.35 x10^{-8}
Agar gel – II	1.2 x10^{-8}
Water – II	1.15 x10^{-8}
Teflon	1.3x10^{-8}

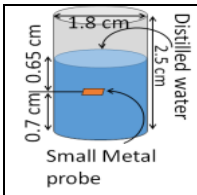

Water-I (Suspended metal probe in it)

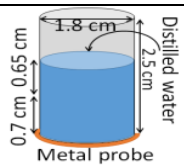

Water-II (no conductor)

Agar gel -I (Probe underneath the agar gel)

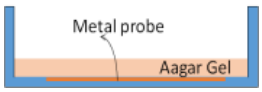

Agar gel -II (Petri dish attached to the probe)

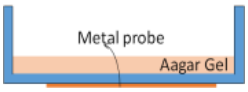

The concentration of hydroxyl (OH) molecule in the plasma-treated water is higher (2.21 µmole/100 µl) when the metal probe is placed inside the water sample than when the probe is kept on the outer surface of the water container (0.746 µmole/100 µl). With the presence of a conductor inside water the amount of generated charge increases, hence changing the plasma-treated water chemistry. It subsequently increases the OH density.

3.2.2 Plasma Spreading pattern on Different Substrates

To observe the plasma spreading pattern on the substrate and the influence of the substrate on the plasma jet and the gas-dynamic, images of the plasma jet were acquired using a digital camera, and the gas flow pattern was studied utilizing the Schlieren imaging technique. The images of the

helium gas jet and the plasma jet in the presence of substrate are shown in figure 5. The digital camera image and the schlieren image are presented parallelly in figures 5a,b,c,e,f,g, and Fig. 5d shows the schlieren image of the plasma jet while it is in contact with water. The digital camera image shows that the plasma jet applies an electrohydrodynamic pressure on the target material. It creates dimples on soft surfaces like agar gel and water (Fig 5a d). The maximum depth created by the plasma jet on the water surface is around 1.5 mm. When the plasma jet is in contact with the metal surface, it creates a bright spot on the surface, which seems like a second discharge starting from the surface. In this case, the free plasma jet also happens to stretch out of the surface, and on the Teflon surface, it creates spikes on the outer radius of the spreading jet. The bright spot diameter on Teflon, agar gel, and metal surface, as measured from the digital camera image is 1.75 mm, 1.5 mm, and 1 mm, respectively (Fig. 5a,b,c). The stagnant laminar flow region is shown in this figure for both Teflon and metal and is 0.8 mm in diameter. Schlieren image (figure 5e,f,g) shows the free gas jet and the effect of the discharge (for three different applied voltages) on the gas jet when the jet is in contact with targets. In all cases, it shows that despite the laminar free gas flow, the discharge creates turbulence around the plasma jet and on the contact surface as in [39]. This turbulence increases with the applied voltage. A higher applied voltage creates a more unstable plasma jet and causes the contact point to fluctuate.

The dynamics of the free gas jet change significantly when the plasma is on. The Schirlen image was taken at the rate of 300 frames per second for 0.16 sec. It shows that when the plasma is “on”, the gas jet moves randomly on the substrate’s surface and the plasma seems to create turbulence in the gas. Therefore, the contact point is not a fixed point on the surface.

The deformation of the gas-liquid interface depends on the pressure gradient across the interface and the interfacial tension [33]. According to Forrester and Evan [40], the crater diameter depends on the height of the nozzle from the surface, gas momentum, and liquid-specific weight. The cavity height increases with the free jet momentum at the contact point and decreases with the diameter of the vessel [40]. The thrust on the surface is the momentum, $M = \rho_g a v^2$ where, a is the cross-sectional area of the jet, ρ_g is the gas density, and v is the gas velocity. Free jet momentum replaces the liquid and the amount of replaced liquid depends on the jet velocity and the surface tension which can be calculated from the equation,

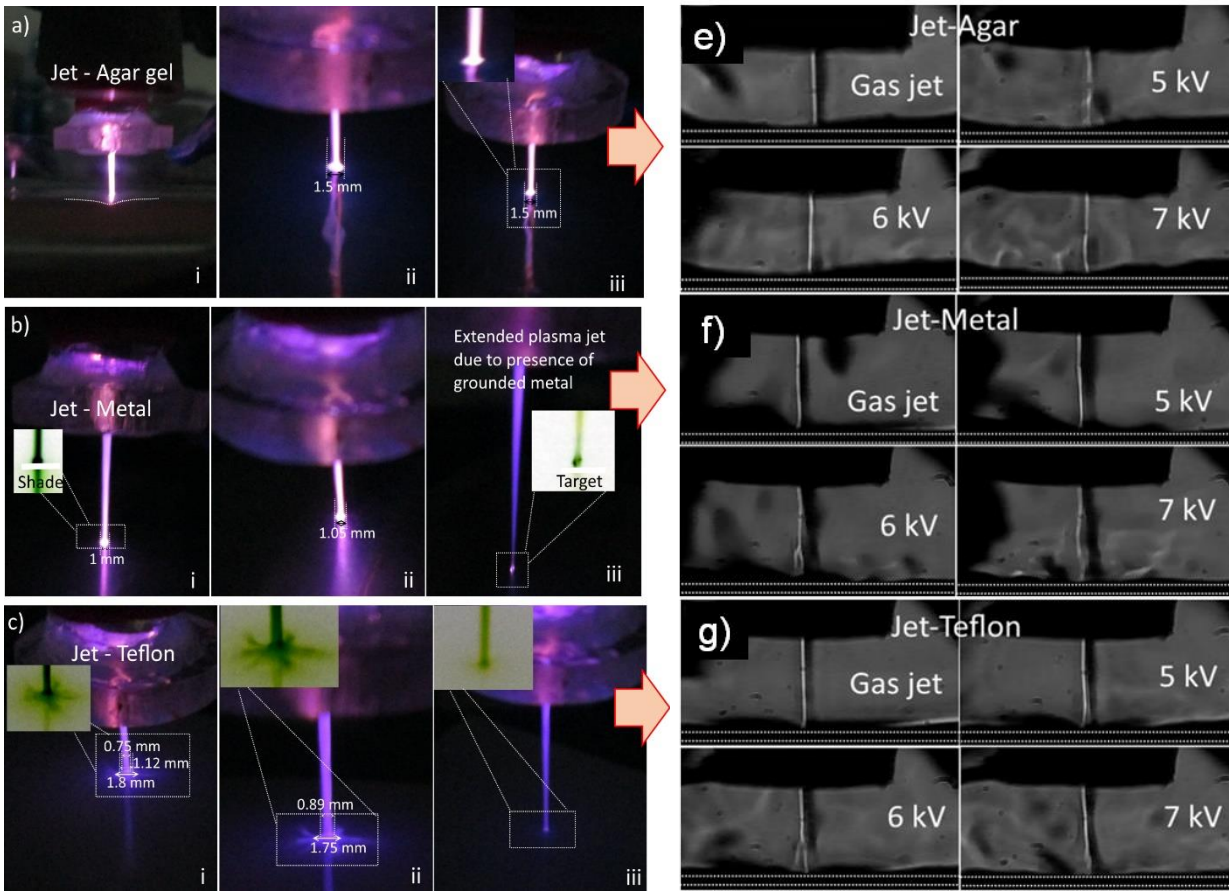

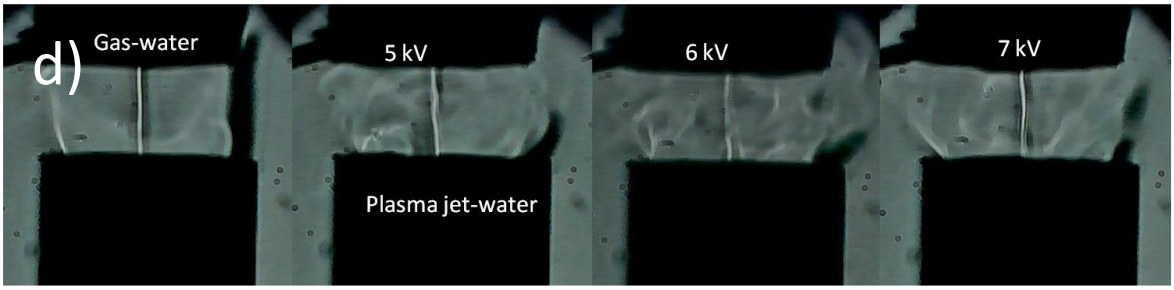

Fig. 5 Digital camera image and schlieren image of the jet impinging on: a,e) Agar gel surface, b,f) Metal surface, c,g) Teflon surface, and d) Water

$\frac{1}{2}\rho_g v^2 = \rho_l g n_0 + \frac{2\sigma}{R_0}$, where ρ_g and ρ_l are the density of gas jet and the liquid (998.2 kg/m^3), v is the jet velocity, g is gravitational acceleration, σ is surface tension (71.97 mN/m), $R_0 = \frac{H^2}{2\beta_* n_0}$ is the radius of curvature of stagnation point and n_0 is the maximum depth on the

liquid surface, β_* depends on the diameter of the nozzle and the height of the nozzle from the liquid surface (*H*).

The thrust on the liquid surface increases with the increase of the surface tension. At 1 cm of the jet axis estimated gas jet velocity is 27 m/s and the gas density ρ_g is 0.125 kg/m^3. The calculated maximum depth is 2.7 mm and the maximum depth as measured from the image of the jet liquid interaction point is 1.41 mm, which is less than the estimated depth. This estimation is done for the gas jet, where the discharge and the reduced radius of the jet are not considered. The jet velocity decreases from the nozzle along the jet axis, therefore, the depth of the liquid surface decreases with the distance between the liquid surface and the nozzle.

3.2.3 Emission intensity of the different species along the jet surface

The emission spectrum from the contact surface was acquired to understand the spreading of the jet plasma on the contact surface. The emission intensity of the different species started from the center of the contact point to the outer surface of the target was tracked (Fig. 6). On the Teflon surface, the intensity of different species is low at the center, and then it increases until 0.8 mm radial position from the center. After this point, it decreases in the radial direction (Fig.6a). The knee of the curve is observed around 1.2 mm radial position. After 2 mm of the radial position, the intensity of different species is too low, and the arbitrary intensity of the different species is almost the same. The intensity of N_2^*, $N_2^{+,}$ and OH is higher than that of He and atomic oxygen (O) near the contact point. For the metal target, at the contact point, the intensity of N_2^* and OH is higher than others and even at the outer surface these intensities are higher than the other species (Fig. 6b). The intensity of the different species is high until the radius of 0.8 mm from the center of the contact point.

On the agar surface, the intensity is unstable and randomly changes near the contact point because the jet creates a dimple on the agar gel at the contact point, so we can acquire the emission spectra of the free plasma jet only. The intensity is high until the radius is 0.6 mm; after that, it decreases very fast. The intensity of N_2^*, OH is higher than N_2^+ (Fig. 6c). In Figure 5, the bright spot radius on the Teflon, the metal surface, and agar gel is 0.87 mm,0.55 mm, and 0.75 mm respectively, whereas the maximum emission intensity is observed approximately until the radius, r =0.8 mm,0.5 mm and 0.6 mm for Teflon, metal surface and agar gel, respectively.

A free gas jet impinging on the solid surface can be subdivided into three regions: i) The free jet region, ii) The stagnant flow region and iii) The region of radial flow. Stagnation flow begins relatively close to the surface and the limiting distance is 1.2 times that of the nozzle diameter [34]. Here, the vertical velocity decelerates, horizontal velocity accelerates, and viscosity's influence is restricted to a thin layer close to the solid surface. The relative boundary layer thickness decreases with the increase of Reynold's number. For real stagnation flow due to the impinging jet of finite diameter, Schrader [35] and Dosdogru [36] calculated the surface velocity component, which increases with the decrease of H/D. Where H is the height of the nozzle from the surface and D is the diameter of the jet. This accelerated stagnation flow becomes the decelerated jet flow on a solid surface. So, the surface parallel velocity initially increases linearly (*velocity* α x) and reaches a maximum value. After that point, the gas jet velocity decreases with the distance (*velocity* α x^{-1}) from that maximum point [34]. In the stagnation region (or accelerating region), the flow is laminar, but immediately after this region, the flow becomes turbulent. The radius of the stagnant region identified in figure 5, depends on the target material and the surface roughness. In our case, the diameter of the gas stagnant region should be 1.2 mm, and it has been observed that around this region (~1.5 mm) the emission intensity of the different species is maximum.

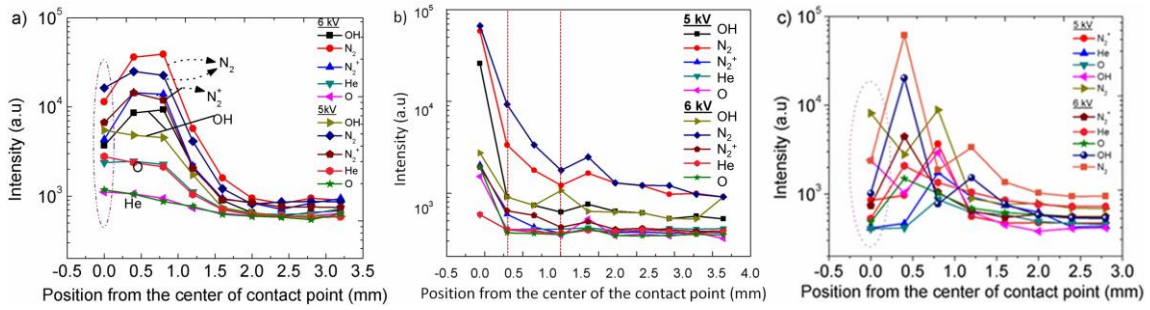

Fig.6 Emission intensity of different species along the substrate's surface: a) Teflon surface, b) metal surface, c) agar gel surface.

4. CONCLUSION

The dynamic behavior of millimeter range plasma jet, its interaction with different materials, and its spreading over the substrates were investigated by employing electrical and optical investigation techniques.

Laminar gas flow regime and the turbulent-free plasma jet length have been estimated from the images, gas flow velocity, and the *Ehd* number. This helps us to identify the position, where the

substrate under treatment can be placed within the laminar region. *Ehd* shows that the turbulence at the plasma jet will be observed at 1.25 cm from the nozzle. This validates our experimental observation. The substrate experiences a force due to the gas flow and this force can deform the shape of the surface. At a gas flow rate of 1.75 slm, the estimated maximum depth created on the water surface is 2.7 mm and the depth measured from the image of the plasma jet-surface interface is 1.4 mm, which is lower than the depth created by feed gas. The gas discharge decreases the dynamic gas pressure on the interface. The plasma jet also creates a depression on the agar-gel surface.

From this study, we have found that the charge passing through the substrate materials plays an important role in surface modification, sample chemistry, and the dynamics of the plasma jet. The charges passing through substrates per voltage pulse are, Agar gel (4.38×10^{-8} C), Metal (4.4×10^{-8} C), Water (2.35×10^{-8} C), and Teflon (1.3×10^{-8} C), these values are higher than the charge that is passing when a dielectric is placed in between the grounded metal probe and the substrate. The porosity of the agar gel makes it more conducting than expected. The OH concentration in the water is higher (2.21 µmole/100 µl) when the grounded conducting probe is placed inside the water sample.

N_2, N_2^+, O, O_2, He, OH, and NO are the main identified plasma species in the plasma jet and on the substrates. The number of plasma species is at the maximum near the contact point and decreases towards the radial surface. On the Teflon surface, the intensity is low at the center of the contact surface and then reaches the maximum, creating a torus-shaped plasma region at the contact point, which is also true for the agar gel (because the plasma jet creates a dimple on the surface). The high-density plasma spreading area is maximum on Teflon and minimum on the metal surface. For an APPJ outlet size of 1 mm, the plasma surface modification area is extended up to 3.5 mm from the contact point. The spread area increases with operating voltage.

From the images of the plasma jet-surface contact point, three different flow regions (free-flow region, stagnant region, and accelerating region) have been identified. The stagnant region is prominent when the plasma jet is in contact with a dielectric material (for Teflon 0.86 mm, and agar gel 0.75 mm), whereas this region is until 0.6 mm for the metal surface, from the center of the contact point. The emission intensity data shows that the higher emission intensity region is within the diameter of 1.6 mm, 1.0 mm, and 1.2 mm on the Teflon, metal, and agar-gel surfaces, respectively. The radius of the stagnant region changes with the target materials, and surface

roughness. The plasma species intensity is higher close to the stagnant region and gradually decreases along the gas accelerating and decelerating area.

REFERENCES:

1. M Yousfi, N Merbahi, A Pathak, and O Eichwald, Low-temperature plasmas at atmospheric pressure: Toward new pharmaceutical treatments in medicine, *Fundam. Clin. Pharmacol*. 28, 123–135 (2014).

2. J F Kolb, A-A H Mohamed, R O Price, R J Swanson, A Bowman, R L Chiavarini, M Stacey, and K H Schoenbach, Cold atmospheric pressure air plasma jet for medical applications, *Appl. Phys. Lett.* 92, 241501–241503 (2008).

3. X Lua, Z Jiang, Q Xiong, Z Tang, X Hu, and Y Pan, An 11 cm long atmospheric pressure cold plasma plume for applications of plasma medicine, *Appl. Phys. Lett*. 92, 081502–081504 (2008).

4. X Zhang, M Li, R Zhou, K Feng, and S Yang, Ablation of liver cancer cells *in vitro* by a plasma needle, *Appl. Phys. Lett*. 93, 021502–021504 (2008).

5. S Banerjee, E Adhikari, P Sapkota, A Sebastian, S Ptasinska, Atmospheric Pressure Plasma Deposition of TiO_2 : A Review. *Materials* 13, 2931 (2020)

6. L Ledwani, J Sangwan Nanotechnology for Energy and Environmental Engineering. Green Energy and Technology, *Springer, Cham.* (2020)

7. Alenka Vesel, Rok Zaplotnik, Gregor Primc, Miran Mozetič. Evolution of the Surface Wettability of PET Polymer upon Treatment with an Atmospheric-Pressure Plasma Jet. *Polymers* 12:1, 87 (2020)

8. Pingshan Luan, Gottlieb S. Oehrlein. Interaction of long-lived reactive species from cold atmospheric pressure plasma with polymers: Chemical modification by ozone and reactive oxygen-nitrogen species. *Journal of Vacuum Science & Technology A* 37:5, 051303 (2019)

9. M Gherardi, N Puač, D Marić, A Stancampiano, G Malović, V Colombo, Z L Petrović, Practical and theoretical considerations on the use of ICCD imaging for the characterization of non-equilibrium plasmas. *Plasma Sources Sci. Technol.* 24, 064004 (2015)

10. S A Norberg, E Johnsen, M J Kushner, Helium atmospheric pressure plasma jets touching dielectric and metal surfaces. *J. Appl. Phys.* 118, 013301 (2015)

11. Vesna V Kovačević *et al* The effect of liquid target on a nonthermal plasma jet—imaging, electric fields, visualization of gas flow and optical emission spectroscopy. *J. Phys. D: Appl. Phys.* 51 065202 (2018)

12. I Schweigert, D Zakrevsky, P Gugin, E Yelak, E Golubitskaya, O Troitskaya, O Koval, Interaction of Cold Atmospheric Argon and Helium Plasma Jets with Bio-Target with Grounded Substrate Beneath. *Appl. Sci.*, 9, 4528 (2019)

13. M Boselli, V Colombo, E Ghedini, *et al.* Schlieren High-Speed Imaging of a Nanosecond Pulsed Atmospheric Pressure Non-equilibrium Plasma Jet. *Plasma Chem Plasma Process* 34, 853–869 (2014)

14. E Robert, V Sarron, T Darny, D Riès, S Dozias, J Fontane, L Joly and J-M Pouvesle, Rare gas flow structuration in plasma jet experiments. *Plasma Sources Science and Technology* 23 (1), 012003 (2014)

15. T Darny, J-M Pouvesle, J Fontane, L Joly, S Dozias and E Robert, Plasma action on helium flow in cold atmospheric pressure plasma jet experiments *Plasma Sources Science and Technology* 26 (10), 105001 (2017)

16. I V Schweigert, S Vagapov, L Lin and M Keidar, Enhancement of atmospheric plasma jet–target interaction with an external ring electrode, *J. Phys. D: Appl. Phys.* 52 295201 (2019)

17. Kim, Myung Chan, Yang, S.H., Boo, Jangho, Han, Ji-Sook, Surface treatment of metals using an atmospheric pressure plasma jet and their surface characteristics, *Surface and Coatings Technology* 174(175):839-844 (2003)

18. A Sobota1, O Guaitella, G B Sretenovi´c, V VKova˘cevi´c, E Slikboer, I B Krstic, B M Obradovi´c, M MKuraica, Plasma-surface interaction: Dielectric and metallic targets and their influence on the electric field profile in a kHz AC-driven He plasma jet, *Plasma Sources Science and Technology*, 28, 4(2019)

19. Gerling T, Nastuta A V, Bussiahn R, Kindel E and Weltmann K D *Plasma Sources Sci. Technol.* 21 034012 ISSN 0963-0252 (2012)

20. A Sobota, O Guaitella, G B Sretenovic, V V Kovacevic, E Slikboer, I B Krstic, B M Obradovic, Plasma-surface interaction: dielectric and metallic targets and their influence on the electric field profile in a kHz AC-driven He plasma jet, *Plasma Sources Science and Technology* 52 17 (2019)

21. Norberg S A, Johnsen E and Kushner M J, Helium atmospheric pressure plasma jets interacting with wet cells: delivery of electric fields, *J. Phys. D. Appl. Phys.* 49 185201 (2016)

22. Darny T, Pouvesle J m, Puech V, Douat C, Dozias S and Robert E, Analysis of conductive target influence in plasma jet experiments through helium metastable and electric field measurements, *Plasma Sources Sci. Technol.* 26 045008 (2017)

23. A V Omran, G Busco, L Ridou, S Dozias, C Grillon, J-M Pouvesle, E Robert, Cold atmospheric single plasma jet for RONS delivery on large biological surfaces. *Plasma Sources Science and Technology* 29 (10), 105002 (2020)

24. R Kakei, A Ogino, F Iwata, M Nagatsu, Production of ultrafine atmospheric pressure plasma jet with nano-capillary. Thin Solid Films, 518 (13), 3457-3460 (2010)

25. A Begum, R Chiba, T Ishijima, M Kakikawa, A Taok, *IEEE Transactions on Radiation and Plasma Medical Sciences* 2 (4), 360-368 (2018)

26. Jun-Seok Oh, Olumuyiwa T Olabanji, Craig Hale, Raffaello Mariani, Konstantinos Kontis and James W Bradley, Imaging gas and plasma interactions in the surface-chemical modification of polymers using micro-plasma jets, *J. Phys. D: Appl. Phys*. 44 155206 (2011)

27. Y Morabit, *et al*, Turbulence and entrainment in an atmospheric pressure dielectric barrier plasma jet, *Plasma Processes and Polymers* 17 (6), 1900217 (2021)

28. Y Morabit, M I Hasan, R D Whalley *et al.* A review of the gas and liquid phase interactions in low-temperature plasma jets used for biomedical applications, *Eur. Phys. J. D* **75**, 32 (2021).

29. T Darny, E Robert, S Dozias and J -M Pouvesle, Helical Plasma Propagation of Microsecond Plasma Gun Discharges, IEEE *Transactions on Plasma Science*, **42**, 10 2506-2507, (2014)

30. T Darny, E Robert, D Riès, S Dozias and J -M Pouvesle, Unexpected Plasma Plume Shapes Produced by a Microsecond Plasma Gun Discharge, IEEE *Transactions on Plasma Science*, **42**, 10, 2504-2505, (2014)

31. S Wu, Z Wang, Q Huang, X Tan, X Lu, and K Ostrikov, Atmospheric-pressure plasma jets: Effect of gas flow, active species, and snake-like bullet propagation *Physics of Plasmas* **20**, 023503 (2013)

32. Begum, Asma. "Experimental Investigation of a Non-Thermal Atmospheric Pressure Plasma Jet" Doctor of Philosophy (Ph.D.), Dissertation, Electrical/Computer Engineering, Old Dominion University, (2010).

33. Theo Van Der Meer, Heat transfer from impinging flame jet, Ph.D. thesis

34. D E Wakelin, The interaction between gas jest and the surface of liquids including molten metals, Ph.D., University of London, UK, 1996.

35. H Schrader, VDI-Forschungsh, 484 (1961).

36. G A Dosdogru, Dissertation, TH Darmstadt, Synopsis in Chem. Ing. Tech. 44 (1972) 1340.

37. Yashuang Zheng, Lijun Wang, Wenjun Ning, and Shenli Jia, Schlieren imaging investigation of the hydrodynamics of atmospheric helium plasma jets, Journal of Applied Physics 119, 123301 (2016)

38. J S Chang and K Urashima, Electrohydrodynamic Gas Flow Regime Map in a Wire-Plate Type Electrostatic Precipitator *InternationalJournal of Plasma Environmental Science and Technology* 3 2 (2009)

39. P K Papadopoulos, P Vafeas, P Svarnas, K Gazeli,P M Hatzikonstantinou, A Gkelios and F Clement, Interpretation of the gas flow field modification induced by guided streamer (‘plasma bullet’) propagation *J. Phys. D: Appl. Phys*. 47 425203 (2014)

40. S E Forrester, G M Evans, Computational modeling study of a plane gas jets impinging onto a liquid pool, International Conference on CFD in Mineral and Metal Processing and Power Generation, Melbourne, pp. 313–320.